

https://dspace.org/

The Feasibility of Electromagnetic Near Field Hotspot Positioning within a Resonant Cavity for Microwave Thermal Ablation

Graeme Young; David Rubin; Alan Clark

https://hdl.handle.net/10539/42925
DOAJ

Downloaded from a DSpace repository. https://dspace.org/

The Feasibility of Positioning Electromagnetic Near Field Hotspots within a Resonant Cavity for Microwave Thermal Ablation

Graeme Young, *Student Member, IEEE*, David Rubin, *SMIEEE*, and Alan Clark, *MSAIEE*

***Abstract*—An investigation into moving electromagnetic near-field hotspots inside a resonant cavity is presented. The investigation focused on simulating an alternative approach to microwave thermal ablation of tumours by manipulating the interaction between electromagnetic near fields instead of utilising an interstitial antenna. The methodology comprised comparing various electromagnetic field solvers, verifying the simulation techniques, characterising a rectangular resonant cavity, and attempting to manipulate the position of its hotspots by introducing a feed phase shift. The effects of dielectric media were also investigated. Progressive hotspot movement was achieved using input phase manipulation between 2.55 and 2.7 GHz with the feeds on opposite walls. No pattern change was evident at the system's eigenfrequencies, indicating a constant field pattern at its resonant peaks. Furthermore, it was determined that the characteristic modes of the system were narrowband, such that the addition of dielectric material altered the system's resonance. Therefore, the application of this method to thermal ablation, which requires high precision, accuracy and control, was deemed impractical. Future recommendations include using adjustable geometry to design field patterns, comparing dielectric media with significant thermal mass, and investigating the 'inverse problem' to create a specific current distribution around the resonant cavity and induce the desired hotspot patterns.**

***Index Terms*—Cavity resonators, electromagnetic fields, frequency domain analysis, microwave theory and techniques, phase control, resonance, thermal analysis.**

I. Introduction

THERMAL ablation of a tumour is the destruction of neoplastic tissue by inducing extreme local hyperthermia or hypothermia [1]. Microwave thermal ablation (MWA) uses the microwave heating effect to induce hyperthermia by directly oscillating water molecules. The method relies on the molecularly polar nature of the water in tumour tissue [1]. Inserting an interstitial needle-like microwave antenna into the body delivers the microwave energy to the tissue. Therefore, the efficacy of the procedure is limited by the location and percutaneous accessibility of the patient's tumour [2]. The electromagnetic near field has unique characteristics in that it is dominated by predominantly reactive components [3]. These wave interactions lead to contrasting areas of high and low electromagnetic field intensity. This configuration can be thought of as a pattern of *hotspots*. If the electric field oscillates at microwave frequencies, the microwave heating effect can be utilised to heat dielectric materials. Microwave radiation is not as easily concentrated and steered as the higher frequency X-band radiation used in radiation therapy. Moreover, to narrow a beam of microwave radiation to a tumour-sized width would require an impractically large antenna. Therefore, the field must be kept in a reactive near-field state and must be bounded by a resonant cavity. This paper outlines an investigation into the feasibility of controlling the positions of near-field hotspots at microwave frequency in a resonant cavity for application in clinical thermal ablation.

Graeme Young was with the University of the Witwatersrand, Johannesburg, South Africa. He is now with Stellenbosch University and the South African Radio Astronomy Observatory (SARAO), Cape Town, South Africa (e-mail: gyoung@sarao.ac.za)

David Rubin is with the University of the Witwatersrand, Johannesburg, South Africa (e-mail: david.rubin@wits.ac.za)

Alan Clark is with the University of the Witwatersrand, Johannesburg, South Africa (e-mail: alan.clark@wits.ac.za)

II. Background

This section discusses thermal ablation, the characteristics of microwaves, and electromagnetic resonance.

A. Thermal Ablation

Thermal ablation destroys tissue by inducing extreme hyper or hypothermia in the tissue as a substitute for open surgery. This is essentially a transient thermal heat transfer problem [4]. There are various implementations of clinical thermal ablation. The most common are radiofrequency ablation (RFA), microwave ablation (MWA), high-intensity focused ultrasound, laser ablation, and cryoablation [5]. MWA and RFA are similar in mechanism; however, MWA operates at a higher frequency. While RFA utilises two electrodes and induces a current between them, MWA creates a pocket of energy, or a hotspot, around the antenna, which interacts with its surroundings. This paper focuses on MWA.

B. Microwaves and the Microwave Heating Effect

Microwaves are electromagnetic waves at microwave frequencies. This range falls between 1 and 100 GHz, corresponding to 300–3 mm wavelengths. The microwave spectrum of frequencies has many applications. Microwave heating is the basis of microwave ovens, which are operated in the *S band* (2–4 GHz), usually centred at 2.45 GHz, fed by imprecise cavity magnetrons. Microwave radiation is classified as non-ionising [6]; heating is achieved by the continuous realignment of polar molecules to the oscillating electric field [7]. Therefore, water-dense tissues are strongly affected and heat up rapidly.

CC BY

1) Dielectric Influence: Different materials exhibit different affinities for converting electromagnetic field energy into heat. This affinity depends on the material's dielectric properties. Each material's capacity to absorb electromagnetic energy is proportional to the ease with which microwaves can penetrate the material [8]. The absorbed energy is then converted into thermal energy. This depends on the dielectric dissipation factor, or loss tangent, represented by $\tan\delta$ [6].

2) Near Field: The area surrounding an electromagnetic source, such as an antenna, is broken up into three regions: the reactive near-field, the radiative near-field and the far-field [3]. This is often approximated to the near-field and the far-field. In the reactive near field, reactive power densities dominate [3]. Many wave interactions result in a fluctuating field pattern, which does not uniformly radiate as a plane wave. This results in areas of increased and decreased magnitude, forming the idea of near-field *hotspots*. The reactive near-field is volatile and prone to mutual coupling.

3) Resonant Cavities: Electromagnetic resonance describes a sharp increase in field strength or magnitude. This results from the application of an electromagnetic force or field of a specific frequency that approaches a natural frequency, or eigenfrequency, of the system upon which it acts [9]. Resonant cavities are bounded resonant structures whose dimensions are comparable with, or larger than, the operating wavelength of the excitation signal. Because these cavities are bounded, they are non-radiative and highly reactive internally. When a cavity is operated at a natural characteristic mode, a near field, high amplitude resonant pattern is evident inside it [10]. These modes also correspond to the maximum power delivery into the cavity.

III. Methodology

The methodology was split into four sections: software benchmarking, model verification, cavity characterisation, and field manipulation.

A. Software Benchmark

A standard benchmark model of a resonant cavity was used to test the simulation software. The programs used were CST Studio Suite [11], FEKO [12] and SuperNEC [13]. These programs cover an array of simulation methods. This section demonstrates how different solvers exhibit different numerical tolerances around resonance. CST utilises the finite element method (FEM) and finite integration technique (FIT), similar to the finite-difference time-domain (FDTD) technique. FEKO uses the standard method of moments (MoM) and the multi-level fast multipole method (MLFMM) as a technique to speed up MoM solutions. It can also use FEM to solve dielectric problems. SuperNEC, an implementation of the numerical electromagnetic code (NEC), uses the MoM. The benchmark model comprised a rectangular resonant cavity with a standard rectangular waveguide feed. The model was designed around a feed frequency of 2.45 GHz. Because a resonant cavity must be comparable with the wavelength of its excitation, its dimensions were chosen as follows: $2\lambda \times 2\lambda \times 1\lambda$. The waveguide cross-section was specified according to standard convention: $0.6\lambda \times 0.3\lambda$. The wavelength of a 2.45 GHz wave is $\approx$ 122.37 mm. Therefore, the cavity dimensions were $244.73 \times 244.73 \times 122.37$ mm. The waveguide was 73.42×36.71 in cross-section and 1λ, or 122.37 mm long. The electromagnetic near fields and radiated power simulations were used to establish a comparison between the programs and inform the best software to proceed with the investigation.

B. Verification

This section describes the method used to verify the results produced by the software. It involved comparing the measured near-field data inside a microwave oven to its simulated field.

1) Measured Field: The fields inside the microwave oven were measured using wet thermal paper (till slip paper). The paper darkens under the influence of heat. Since the microwave heating effect acts upon polar molecules like water, the paper was dampened so the heated water would darken the paper. Strips of the paper were attached to square sheets of polystyrene, which were placed inside the microwave oven. The oven under test was the Defy DMO 383 Microwave Oven.

2) Operating Frequency: Cavity magnetrons deliver energy to microwave ovens. The operating frequency of a magnetron is not precise and is variable. This frequency change is partly influenced by 'pulling' and 'pushing' on the magnetron from changes in the reflected power and internal cathode current. Radiated microwave leakage from the oven was measured to determine the range of frequencies over which the magnetron operates. A log-period dipole array (LPDA) was used to measure the radiation emanating from the operating oven in an anechoic chamber.

3) Simulation: An accurate theoretical model was created to simulate the near fields. FEKO was the only field solver used for this, as it was the only program with a license that allowed for enough mesh cells. The geometry of the cavity was measured and modelled in Computer Aided Design (CAD) as a perfect electric conductor (PEC). The dielectric polystyrene slab used to support the paper was added to the model. Simulations were then conducted over the magnetron's operating frequency range. The solver was set up to use the MoM for the cavity and FEM for the dielectric interactions.

4) Comparison: The measured and simulated data were compared graphically through image processing. Photographs of the measured patterns were taken. These were cropped to square, converted to a *double* format, and grayscaled. Then, a pixel intensity threshold was set and applied to create a binary image. Finally, the logical OR operator was applied to all the images to provide the loci of all measured hotspots. A similar operation was conducted for the simulated near field patterns. This enabled a direct comparison of the measured and simulated hotspot positions.

C. Cavity Characterisation

This section discusses the characterisation of a rectangular cavity and waveguide resonator simulation model to be used to test phase shift methods and examine the near-field hotspots.

1) Model Design: The model was designed on documented rectangular waveguide characteristics. The standard waveguide WR340 is ideally suited to microwave applications. It has a recommended operating bandwidth of 2.20–3.30 GHz, which includes the conventional microwave frequency of 2.45 GHz and accounts for variance. The cavity's dimensions were designed at a scalar multiple of the WR340 waveguide dimensions. A TE_{303} standing wave pattern was designed for. This is represented by a 3×3 grid of hotspot columns. Hence, the cavity dimensions were chosen to be triple the waveguide dimensions. The WR340 waveguide is 86.36×43.18 mm in cross-section. Therefore, the cavity dimensions were $259.08 \times 259.08 \times 129.54$ mm.

2) Cavity Resonance: The dominant characteristic modes of a rectangular resonant cavity can be calculated analytically using (1) [14]. $\sqrt{\mu_r \epsilon_r} = 1$ for free space problems.

$$f_{mnl} = \frac{ck_{mnl}}{2\pi\sqrt{\mu_r \epsilon_r}} \tag{1a}$$

$$k_{mnl} = \sqrt{\left(\frac{m\pi}{a}\right)^2 + \left(\frac{n\pi}{b}\right)^2 + \left(\frac{l\pi}{d}\right)^2} \tag{1b}$$

Where:

f_{mnl} = resonant frequency for mode TE_{mnl} [Hz]
k_{mnl} = wave number for mode TE_{mnl}
c = speed of light [$2.998m \times \cdot s^{-1}$]
a, b, d = dimensions of the cavity [m]

(1) was used for both the cavity and the waveguide feed, as a waveguide can be thought of as a cavity in itself. HFWorks [15] was used to verify the modal calculations for the waveguide. The near-fields inside the cavity were simulated in CST and FEKO around each of the calculated characteristic modes.

3) Dielectric Interaction: A cylinder of water was added to the model. The near fields were simulated and examined. The radiated power into the cavity was compared to the empty cavity. Additionally, the voltage standing wave ratio (VSWR) of the system was considered. The water provides an absorbing body that would alter the resonating behaviour of the cavity. Additionally, the bandwidths of the characteristic modal frequencies were investigated.

D. Field Manipulation

Input phase shift was investigated to manipulate the field and reposition the system's hotspots. Another waveguide was added to the model. The two waveguides were placed in various orientations, facing in different relative directions. They were placed on the same cavity face, adjacent faces, and opposite faces. This represents 0°, 90° and 180° relative geometric phase difference. The waveguides were then fed with progressively differing phases, creating a phase shift between them. The phase shift was increased incrementally, and hotspot movement was sought. An increment of 15° was used between 0° and 360°, resulting in 24 iterations of phase difference.

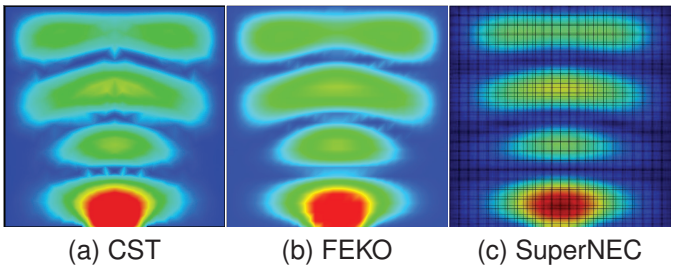


Fig. 1. Benchmark Comparison in CST, FEKO and SuperNEC. These simulations show a horizontal slice through the near-field pattern in a simple resonant cavity model. Blue indicates minimum electric field strength, while red indicates maximum field strength.

IV. Results

The results of the investigation methodology are discussed in this section.

A. Benchmark Model

The near-field pattern in the horizontal plane was the metric used to compare the programs. The result of the benchmark simulation is shown in Fig. 1, displaying a near-identical field pattern elicited from CST and FEKO, with a similarity to SuperNEC's result. CST and FEKO use a waveguide port feed mechanism, whereas SuperNEC uses a monopole feed, accounting for the difference in result. Because FEKO and SuperNEC used a MoM solver, their power and average electric near-field strength were compared. Two SuperNEC models were compared to the FEKO model. The waveguide in the second NEC model was elongated to emulate a plane wave. For FEKO and the first NEC model, a radiated power ratio of $\approx 69:1$ and a voltage ratio of $\approx 7.6:1$ was evident. This indicates a power-to-voltage ratio of $\approx 9.1:1$. For FEKO and the second NEC model, a power ratio of $\approx 238:1$ and a voltage ratio of $\approx 24.8:1$ was evident, indicating a power-to-voltage ratio of $\approx 9.6:1$. The similar ratios indicate that different feed mechanisms for a given model and solver result in a linear field scaling factor. The consistent factor speaks to validity, further proving that the different programs yield similar results.

B. Verification

The operational frequency range of the microwave oven was measured using a spectrum analyser connected to an LPDA inside the shielded anechoic chamber at Wits University. A resolution bandwidth of 300 kHz and a frequency range of 2.25–2.75 GHz were used. Various tests were conducted with only a slab of polystyrene in the oven. The result of the investigation is shown in Fig. 2, indicating that the microwave's magnetron operates predominantly between 2.4 and 2.5 GHz.

Based on the determination of the microwave's operational frequencies, the model simulation focused mainly on the 2.4–2.5 GHz range, with coarse simulations spanning 2.2–2.7 GHz. The field patterns within that range were compared to the measured fields. 12 measurements were conducted to measure the near fields inside the microwave oven. The 3 clearest

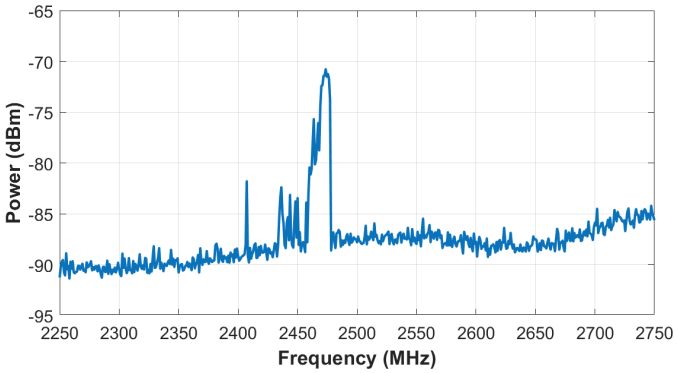
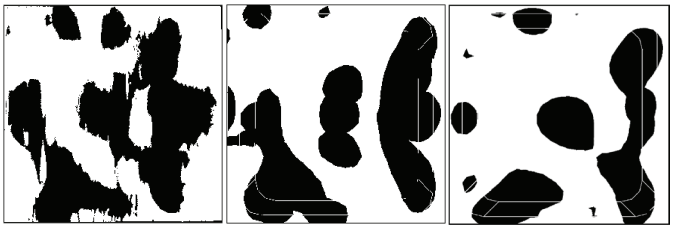


Fig. 2. Microwave Oven External Radiated Power Measured in an Anechoic Chamber.



(a) Measured Microwave Hotspots (b) 2.44–2.5 GHz FEKO Simulation (c) 2.33–2.35 GHz FEKO Simulation

Fig. 3. Comparison of Measured and Simulated Binary Images. The comparison shows the relative locations of the microwave hotspots in each context.

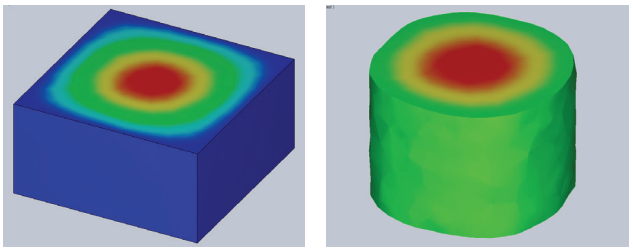
images were selected and processed. The best matching range was 2.44–2.5 GHz. Within the range, 4 major patterns were evident at 2.442, 2.459, 2.489, and 2.497 GHz. Another similar pattern was evident outside the determined range, at 2.33–2.35 GHz, using a polystyrene dielectric model with different properties. The images of these field patterns were processed to create binary images like the measured images. Fig. 3 shows a comparison of the binary hotspot images. The binary images create a platform where like-for-like hotspot positions are discernible. The demonstrated similarity between the simulations and the measured results verifies FEKO's simulation for the application. From Fig. 1, which indicates approximate identical results between CST and FEKO, it was concluded that both programs were suitable to proceed with the investigation.

C. Characterisation

This section presents the results of characterising the *ideal* model.

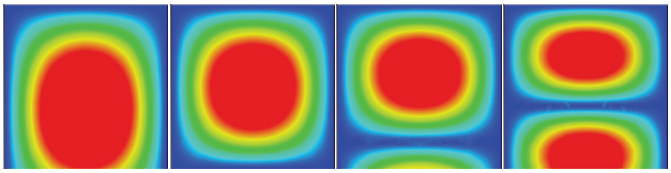
1) Waveguide Resonator: It was analytically determined that the WR340 waveguide resonates at 2.4547 GHz, using (1). This corresponds to characteristic mode TE_{101}. The resonance study in HFWorks, shown in Fig. 4, demonstrated that the waveguide resonates at 2.4539 GHz, which is within 1 MHz of the analytical value.

The frequency sweep in CST shows modal behaviour in the waveguide's recommended operating band of 2.2–3.3 GHz, as depicted in Fig. 5. This demonstrates that mode TE_{10} dominates between 2.2–2.7 GHz. At 3.3 GHz, TE_{20} starts



(a) No Clipping (b) Iso Clipping

Fig. 4. Electric Near Field of WR340 Waveguide at 2.4539 GHz in HFWorks.



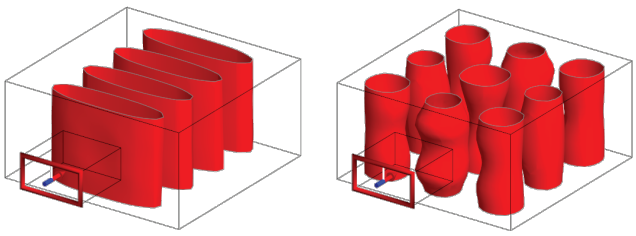
(a) 2.2 GHz (b) 2.45 GHz (c) 2.7 GHz (d) 3.3 GHz

Fig. 5. Excitation of WR340 Waveguide in CST. Blue indicates minimum electric field strength and red indicates maximum electric field strength.

dominating, confirming that 2.2–2.7 GHz is the practical simulation frequency range.

2) Cavity Resonance: The resonance of the cavity depends on the excitation of the waveguide. However, the cavity's geometry implies natural eigenfrequencies, which were calculated using (1). The calculation yielded 18 different transverse electric characteristic modes at 4 different frequencies: 2.3856, 2.4547, 2.5875 and 2.6514 GHz, for the ideal rectangular cavity. The addition of rectangular waveguides influences the natural resonance of the system as the geometry is altered. The patterns of the characteristic modes were simulated, and the first two are shown in Fig. 6. The frequencies at which the resonant peaks were simulated correspond to the analytically calculated values. Because the cavity has a square base design, a characteristic mode can be described by several modes. TE_{104}, TE_{303} and TE_{122} were the most dominant patterns. These are the system's resonant frequencies.

3) Bandwidth: FEKO was used to simulate the radiated power at the waveguide port entering the cavity. Fig. 7 depicts peaks at the expected frequencies. The resonant peaks are



(a) Eigenmode 1 - TE_{104} - 2.386 GHz (b) Eigenmode 2 - TE_{303} - 2.454 GHz

Fig. 6. Characteristic Modes of the Resonant Cavity. These are 3D binary images indicating areas of field strength exceeding a threshold (shown in red). The fields were simulated in FEKO.

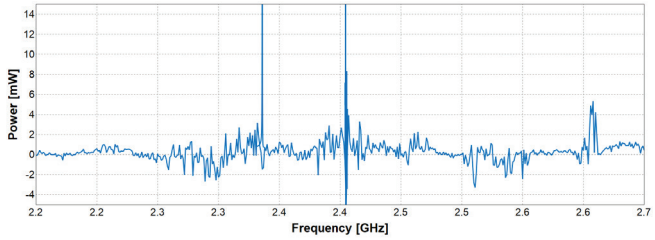


Fig. 7. Radiated Power from the Waveguide Port in the Resonant Cavity. Simulated in FEKO.

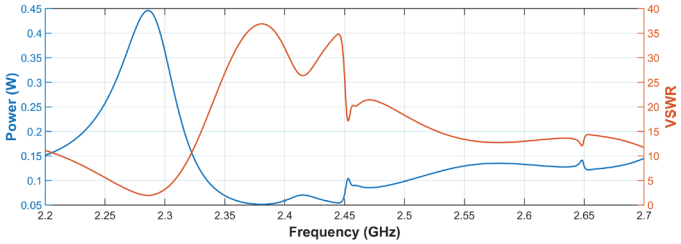


Fig. 8. Power and VSWR in the Resonant Cavity with the Addition of Water, an Absorbing Dielectric. Simulated in FEKO.

shown to be narrowband, in the order of 100–200 kHz. This demonstrates the sensitivity of the resonance within the cavity.

4) Dielectric Influence: The addition of the cylinder of water introduced an absorbing body into the cavity. This made it possible to investigate the system's VSWR. VSWR and power were both simulated. These are shown in Fig. 8. The power curve exhibits higher stability and no resonant peaks, indicating the high dielectric sensitivity inherent to resonant systems.

D. Phase Manipulation

Three models were investigated for phase shift response. Model 1, with two waveguides spaced evenly on the same face of the cavity; model 2, with waveguides placed centrally on adjacent faces of the cavity; and model 3, with waveguides placed centrally on opposite faces of the cavity. The system's eigenfrequencies shifted as a result of the additional waveguide to the cavity. The feed phase did not affect hotspot movement at each characteristic mode; only the electric field strength was affected. This is shown in Fig. 9, which depicts the phase difference at the 2nd resonant peak for model 1. The same is true for all resonant peaks for all models. All figures pertaining to the feed's phase indicate a colour plot that maps electric field strength within the cavity, with blue indicating the minimum field strength and red indicating the maximum field strength.

1) Model 1: For non-resonant frequencies, interference patterns were observed. For model 1, the waveguides are geometrically in phase. Fig. 10 shows the effect of phase shifting the feeds. The pattern at 2.419 GHz was selected for presentation and is indicative of the other non-resonent frequency spans. The plot indicates no hotspot movement; the pattern remains unchanged at most phase shifts. At 180°feed phase shift, the field exhibits destructive interference and cancels itself out. Additionally, it was observed that the field

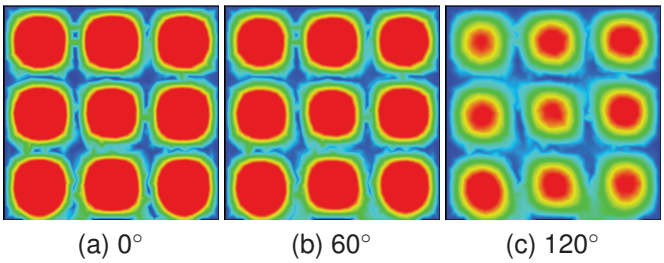


Fig. 9. Effect of feed phase at 2.4478 GHz, the 2nd characteristic mode, for Model 1. Simulation generated by CST Studio Suite.

was symmetrical in this pattern. This plane of symmetry is described by the symmetry of the model.

2) Model 2: The simulations of model 2 exhibited similar characteristics. Because the waveguides' relative geometric phase difference was 90°, the patterns were symmetrical about 90°of electrical phase difference. This is shown in Fig. 11. The presentation frequency selected was 2.385 GHz. As with model 1, the result yielded no progressive hotspot movement, only a near-field pattern *flip* about the electric axis of symmetry. In this case, the field strength does not exhibit destructive interference at the crossover point of 90°.

3) Model 3: In model 3, the waveguides were geometrically out of phase at 180°difference. Therefore, a feed phase shift of 180°results in an in-phase cavity feed. Fig. 12 shows model 3's near-field pattern at 2.599 GHz as a function of phase shift. The pattern shows a single central hotspot which progressively shifts towards the lagging waveguide feed as phase shift is increased from 90°to 270°. At 180°phase shift, when the excitation is in phase, the hotspot is localised to the centre of the cavity. This movement was inherent at all simulated frequency points in the 2.588–2.7 GHz range, bar the resonant peak at 2.651 GHz. This simulation indicates a positive result of the investigation and demonstrates that controlling the position of near-field hotspots within a resonant cavity is theoretically possible.

E. Feasibility

The simulations indicated that controlling the hotspot positions in a resonant cavity is theoretically possible, as demonstrated in Fig. 12, under specific circumstances. This occurred only for model 3 in a specific frequency band, excluding the resonant peaks. At resonant peaks, the bandwidth of the system was narrow, in the order of 100–200 kHz, discussed in *Section IV-C3.* Additionally, in *Section IV-C4*, dielectric bodies were determined to influence the resonant behaviour of the system, altering the presence and the frequency of resonant peaks and the system's stability. This indicates that the resonance in a resonant cavity is volatile and sensitive to changing conditions. Altering dielectric media in the cavity means the system resonates differently. Therefore, it was concluded that resonant near-field manipulation is not feasible for applications in the highly precise field of thermal ablation.

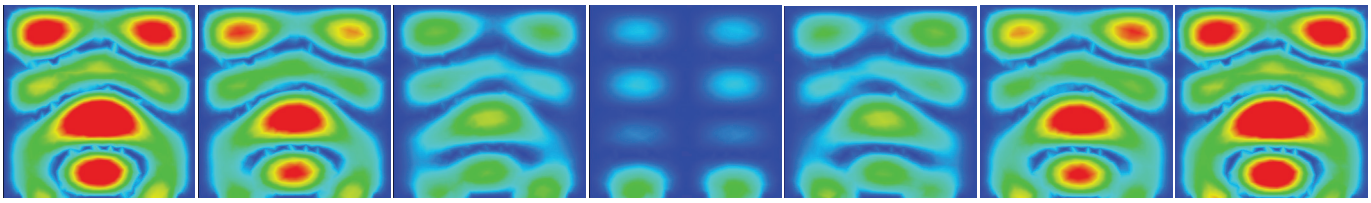


Fig. 10. Simulated colourmap of the EM near-field depicting the hotspot positions as a function of phase shift at 2.419 GHz for Model 1. Simulation generated by CST Studio Suite.

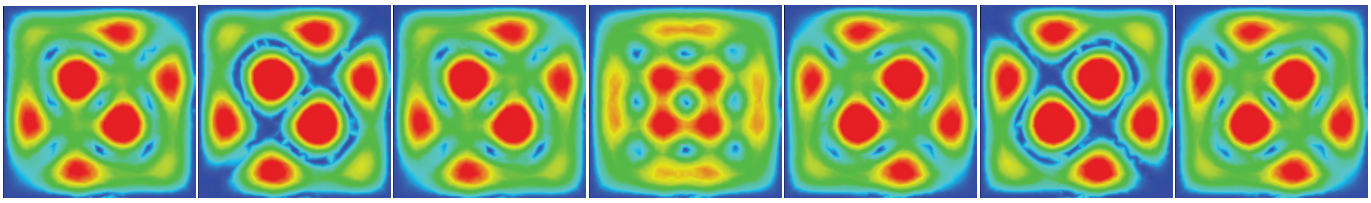


Fig. 11. Simulated colourmap of the EM near-field depicting the hotspot positions as a function of phase shift at 2.385 GHz for Model 2. Simulation generated by CST Studio Suite.

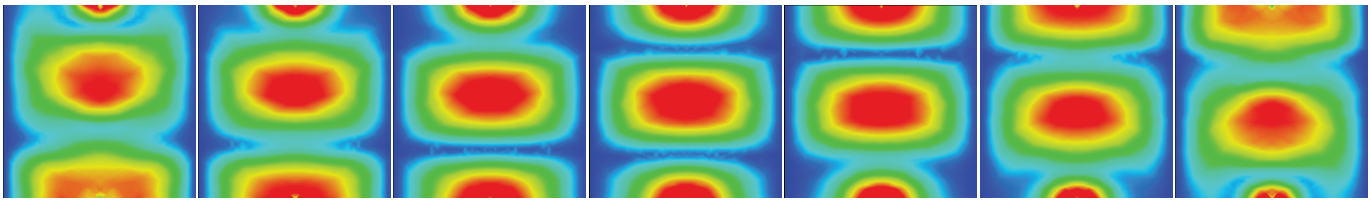


Fig. 12. Progressive Hotspot Movement as a Result of Shifting the Feed Phase Difference at 2.599 GHz for Model 3. This hotspot movement represents the single positive outcome of the investigation.

V. Future Recommendations

In this investigation, the electrical input phase of the system was controlled to move near field hotspots. Geometric control could also be utilised. Moreover, the 'inverse problem' could be considered in the future. Whereby the current distribution induced on a surrounding metallic surface by an ablation antenna is calculated and then induced to the surface of an identical surface, effectively recreating the initial pattern created by the ablation antenna. Furthermore, the positive result achieved during the investigation could be explored, with a broader focus on dielectric influence, and expanded to include larger cavities with multiple primary hotspots.

VI. Conclusion

The investigation presented in this paper aimed to determine whether the position of electromagnetic hotspots inside a resonant cavity could be consistently controlled using feed phase manipulation and whether such a method is feasible for the thermal ablation of tumours. It was concluded that while theoretically, the hotspot positions could be controlled under certain circumstances, this approach, as outlined in the investigation, is not feasible for use in high precision and unique applications like microwave thermal ablation. Future work could include a broader investigation of the dielectric influence on the positive simulation result.

Acknowledgment

The authors would like to acknowledge the University of the Witwatersrand for supplying the resources needed to conduct this investigation, particularly the FEKO license, which was paramount to the research. Additionally, they would like to acknowledge Dassault Systèmes for providing a student edition of CST Studio Suite, an integral program throughout the investigation; and EMWorks for providing a student evaluation of HFWorks.

References

[1] C. Brace, "Thermal tumor ablation in clinical use," *IEEE Pulse*, vol. 2, no. 5, pp. 28–38, Sep. 2011.

[2] L. S. Poulou, E. Botsa, I. Thanou, P. D. Ziakas, and L. Thanos, "Percutaneous microwave ablation vs radiofrequency ablation in the treatment of hepatocellular carcinoma." *World journal of hepatology*, vol. 7, pp. 1054–63, May 2015.

[3] C. A. Balanis, *Antenna Theory, Analysis and Design*, 4th ed. John Wiley & Sons, Inc., 2016, ch. 2, pp. 25–127.

[4] N. T. Wright, "Quantitative models of thermal damage to cells and tissues," in *Heat Transfer and Fluid Flow in Biological Processes*, S. M. Becker and A. V. Kuznetsov, Eds. Boston: Academic Press, 2015, ch. 3, pp. 59 – 76.

[5] D. Dupuy and M. Shulman, "Current status of thermal ablation treatments for lung malignancies," *Seminars in interventional radiology*, vol. 27, pp. 268–75, 09 2010.
[6] P. A. Mello, J. S. Barin, and R. A. Guarnieri, "Microwave heating," in *Microwave-Assisted Sample Preparation for Trace Element Analysis*, Érico Marlon de Moraes Flores, Ed. Amsterdam: Elsevier, 2014, ch. 2, pp. 59 – 75.
[7] J. Tang and F. Resurreccion, "Electromagnetic basis of microwave heating," in *Development of Packaging and Products for Use in Microwave Ovens*, M. W. Lorence and P. S. Pesheck, Eds. Woodhead Publishing, 2009, ch. 1, pp. 3 – 38e.
[8] L. Campañone, C. Paola, and R. Mascheroni, "Modeling and simulation of microwave heating of foods under different process schedules," *Food and Bioprocess Technology*, vol. 5, pp. 738–749, 01 2011.
[9] L. P. Kollár and G. Tarján, "Basics of vibration," in *Mechanics of Civil Engineering Structures*, ser. Woodhead Publishing Series in Civil and Structural Engineering, L. P. Kollár and G. Tarján, Eds. Woodhead Publishing, 2021, ch. 8, pp. 299–343.
[10] M. Mehdizadeh, "Fundamentals of field applicators and probes at radiofrequencies and microwave frequencies," in *Microwave/RF Applicators and Probes*, 2nd ed., M. Mehdizadeh, Ed. Boston: William Andrew Publishing, 2015, ch. 2, pp. 34–67.
[11] "Cst studio suite - free electromagnetic simulation software," https://www.3ds.com/products-services/simulia/products/cst-studio-suite/student-edition/, Dassault Systèmes SE, [Online] Accessed: 2021-04-30.
[12] Altair, "Altair feko," https://www.altair.com/feko/, [Online] Accessed: 2021-04-30.
[13] D. Nitch, *SuperNEC: MOM-UTD Hybrid User Reference Manual*, Poynting Software (Pty) Ltd.
[14] D. M. Pozar, *Microwave Engineering*, 4th ed. John Wiley & Sons, Inc., 2012, ch. 6, pp. 284–287.
[15] EMWorks, "Hfworks - antenna and electromagnetic simulation software," https://www.emworks.com/product/hfworks, [Online] Accessed: 2021-07-01.



Graeme R. Young is currently pursuing a Ph.D in Electronic Engineering at Stellenbosch University, South Africa. He received his B.Eng.SC in Biomedical Engineering in 2017, B.Sc.(Eng) in Electrical Engineering in 2019, and his MScEng in Electronic Engineering in 2021 from the University of the Witwatersrand, South Africa. His current research involves noise and nonlinear distortion in radio receiving systems. He works on receiver development for the Radio Frequency Interference team at the South African Radio Astronomy Observatory in Cape Town, South Africa. He is a student member of the IEEE. His research interests include electromagnetics, RF systems, antennas and biomedical engineering.



Prof. Alan R. Clark attained the degrees of B.Sc.(Eng) and Ph.D. in Electrical engineering in 1987 and 1993 from the University of the Witwatersrand, Johannesburg. He lectured at the same institution from 1990, and was promoted to Associate Professor in October 2002. He has served as an Assistant Dean in the Faculty of Engineering from 2007 to date. Alan has graduated twenty-one M.Sc. and two Ph.D. postgraduates. He is a member of the South African Institute of Electrical Engineers. His research interests are in the field of computational electromagnetics, with particular emphasis on improving a Method-of-Moments code: SUPERNEC; general antenna design; simulation and measurement techniques; and Electromagnetic Compatibility.



Prof. David M. Rubin received his medical degree from the University of Pretoria. He has a Diploma in Anaesthetics and a Fellowship in Nuclear Medicine from the Colleges of Medicine of South Africa, and holds a Masters in Biomedical Engineering from the University of New South Wales, and a Master of Medicine from the University of the Witwatersrand, Johannesburg. He has worked as a clinician and specialist in Nuclear Medicine, after which he founded the Biomedical Engineering Research Group at the University of the Witwatersrand, Johannesburg, which he currently leads as Adjunct Professor in the School of Electrical and Information Engineering. His research interests include medical education and developments at the interface of medicine and engineering.

CONTENTS PAGE